Quaternary Science Reviews 366 (2025) 109504

Contents lists available at ScienceDirect

Quaternary Science Reviews

journal homepage: www.elsevier.com/locate/quascirev

A 150,000-year lacustrine record of the Indo-Australian monsoon from northern Australia

Michael I. Bird [a,b,g,*], Michael Brand [a,b], Rainy Comley [a,b,g], Xennephone Hadeen [a,b], Zenobia Jacobs [b,c], Cassandra Rowe [a,b,g], Frédérik Saltré [b,d,e,f,g], Christopher M. Wurster [a,b,1], Costijn Zwart [a], Corey J.A. Bradshaw [b,d,g]

[a] College of Science and Engineering, James Cook University, Cairns, Queensland, 4870, Australia
[b] Australian Research Council Centre of Excellence of Australian Biodiversity and Heritage, Wollongong, New South Wales, Australia
[c] Centre for Archaeological Science, School of Earth, Atmospheric and Life Sciences, University of Wollongong, Wollongong, New South Wales, 2522, Australia
[d] Global Ecology | Partuyarta Ngadluku Wardli Kuu, College of Science and Engineering, Flinders University, GPO Box 2100, Adelaide, South Australia, 5001, Australia
[e] Biogeography Ecology & Modelling, School of Life Sciences, University Technology Sydney, Sydney, New South Wales, 2007, Australia
[f] Australian Museum Research Institute, Australian Museum, Sydney, New South Wales, 2010, Australia
[g] Australian Research Council Centre of Excellence for Indigenous and Environmental Histories and Futures, Cairns, Queensland, Australia

ARTICLE INFO

Handling Editor: P Rioual

Keywords:
Monsoon
Quaternary
Megalake
Drought
Flood
Atlantic meridional overturning circulation
Vegetation response

ABSTRACT

Nearly two thirds of the world's population depend on monsoon rainfall, with monsoon failure and extreme precipitation affecting societies for millennia. Monsoon hydroclimate is predicted to change as the climate warms, albeit with uncertain regional trajectories. Multiple glacial-interglacial terrestrial records of east Asian monsoon variability exist, but there are no terrestrial records of equivalent length from the coupled Indo-Australian monsoon at its southern limit — Australia. We present a continuous 150,000-year lacustrine record of monsoon dynamics from the core monsoon region of northern Australia based on the proportion of dryland tree pollen in the total dryland pollen spectra and the hydrogen isotope composition of long chain *n*-alkanes. We show that rainfall at the site depends strongly on sea level, which changes proximity of the coast to the site by 320 km over the last glacial-interglacial cycle. Long-term trends in rainfall are broadly anti-phased with the east Asian monsoon modulated by coastal proximity. The record also contains multiple, short intervals (~2 to < 10,000 years) of large changes in tree cover (from 5 to 95 % tree pollen over 3000 years in one instance). Changes in tree cover are frequently but not always, accompanied by synchronous large changes in the other hydroclimate proxies. While these wetter periods cannot be easily ascribed to orbitally induced changes in insolation or coastal proximity, they are correlated with most Heinrich events. This relationship implies that strong asymmetry in inter-hemispheric monsoon rainfall might be one outcome of the current weakening in the strength of the Atlantic meridional overturning circulation, through a reduction in oceanic heat transfer from the Southern to the Northern Hemisphere.

1. Introduction

The dominant feature of climate across most of the tropics and subtropics is a seasonal reversal of the prevailing winds across the Equator, resulting in a wetter summer season and a drier winter in each hemisphere. At an annual scale, the 'global monsoon', approximated hydrologically by the zone of maximum rainfall associated with the intertropical convergence zone, oscillates between the Northern and Southern Hemispheres (An et al., 2015; Wang et al., 2017). This oscillation is driven by the annual cycle of maximum insolation between each hemisphere (Deininger et al., 2020), leading to anti-phased summer rainy seasons in each (Eroglu et al., 2016; Deininger et al., 2020). Agriculture and ecosystems across the tropics and subtropics depend on monsoon rainfall (An et al., 2015), and so growing populations and climate change increase vulnerability to any change in monsoon dynamics (Zhang et al., 2018; Martinez-Villalobos and Neelin, 2023).

* Corresponding author. College of Science and Engineering, James Cook University, Cairns, Queensland, 4870, Australia.
E-mail address: michael.bird@jcu.edu.au (M.I. Bird).
[1] Current address: Isotrace NZ Ltd, 167 High St, Dunedin, New Zealand.

https://doi.org/10.1016/j.quascirev.2025.109504
Received 23 April 2025; Received in revised form 23 June 2025; Accepted 23 June 2025
Available online 9 July 2025

Indeed, drought associated with monsoon failure, as well as monsoon-related flooding, have driven major demographic changes in prehistory (e.g., Cook et al., 2010) and the recent past (Li et al., 2011; Qian et al., 2012; Wang et al., 2015).

The monsoon system that affects the largest land area and human population is the east Asian summer monsoon north of the Equator, coupled by cross-equatorial airflow to the Indo-Australian summer monsoon south of the Equator (Li and Li, 2014) (Fig. 1). This region extends from China through Southeast Asia, the maritime continent and western Indo-Pacific warm pool on the Equator, to Australia. The region is home to almost a billion people and five terrestrial biodiversity hotspots (Myers et al., 2000).

The Indo-Australian summer monsoon represents the dominant source of rainfall in northern Australia, although atmospheric teleconnections to other sources of global interannual climate variability, particularly El Niño-Southern Oscillation, contribute to rainfall variability (Sharmila and Hendon, 2020; Heidemann et al., 2023; Gallagher et al., 2024). The Indo-Australian summer monsoon in northern Australia also exhibits its own internal dynamics, due in approximately equal measure to local oceanic (sea surface temperature, evaporation, and wind) and terrestrial (land cover, soil moisture, evaporation, and wind) influences on rainfall (Yu and Notaro, 2020; Sekizawa et al., 2021; Heidemann et al., 2023; Sekizawa et al., 2023). While the east Asian summer monsoon is dominant due to the large, high-altitude Asian landmass, the internal dynamics of the Indo-Australian summer monsoon can also drive variability in east Asian winter monsoon rainfall in southern China, suggesting close linkages (Yu and Notaro, 2020; Sekizawa et al., 2021; Heidemann et al., 2023; Sekizawa et al., 2023).

Terrestrial speleothem oxygen isotope and pollen records (e.g., Ma et al., 2023; Chen et al., 2023) spanning one or more glacial-interglacial cycles have demonstrated periods of enhanced/(reduced) east Asian summer monsoon rainfall at times of higher/(lower) Northern Hemisphere insolation and distinct, weak monsoon intervals, some of which are coincident with Heinrich events (Cheng et al., 2009, 2016). However, equivalent long terrestrial records from the southern end of the Indo-Australian summer monsoon in northern Australia are conspicuously absent.

Proxy records of terrestrial runoff have been derived from marine records off north-western Australia and are correlated with east Asian summer monsoon records (Pei et al., 2021; Zhang et al., 2020; Sarim et al., 2023) (Fig. 1). However, those records are potentially confounded by the adjacent wide continental shelf that introduces an effect of sea-level change at orbital timescales on the delivery of runoff-derived sediment to the core locations. The locations are also likely affected by the large changes in land-sea distribution in the maritime continent that modify heat and mass transfer through the Indonesian throughflow upstream of the core sites (Lee et al., 2019). On land, a discontinuous speleothem time series of oxygen isotope has been generated covering the last 40 kyr (1 kyr = 1000 years) from northern Western Australia (Denniston et al., 2017), a location that is under the influence of the 'pseudo' monsoon (Suppiah, 1992; Gallagher et al., 2024) where airflow originates in the eastern Indian Ocean, rather than from equatorial regions to the north (Fig. 1).

In the arid interior of Australia, sediments from the former Woods and Gregory 'megalakes' (now small, ephemeral bodies of water) show that large perennial water bodies existed, dominantly during periods in Marine Isotope Stage (MIS) 3 around ~ 50 ka ago, MIS 5 around 100 ka ago, as well as earlier (Bowler et al., 1998, 2001; Veth et al., 2009; Fitzsimmons et al., 2012). These megalakes were fed by monsoon rain falling into south-draining catchments, with drainage divides at least 300 km south of the modern north Australian coast (Fig. 1). Kati Thandi-Lake Eyre in central Southern Australia receives water from the core monsoon area (and other regions), but it also contains a record of megalake periods through MIS 5 to ~ 116 ka ago and from 65 to 45 ka ago (Cohen et al., 2022).

The existence of interior megalakes, orders of magnitude larger than today's, implies past periods of higher monsoon rainfall penetrating these arid interior catchments (Wyrwoll and Valdes, 2003). Debate on

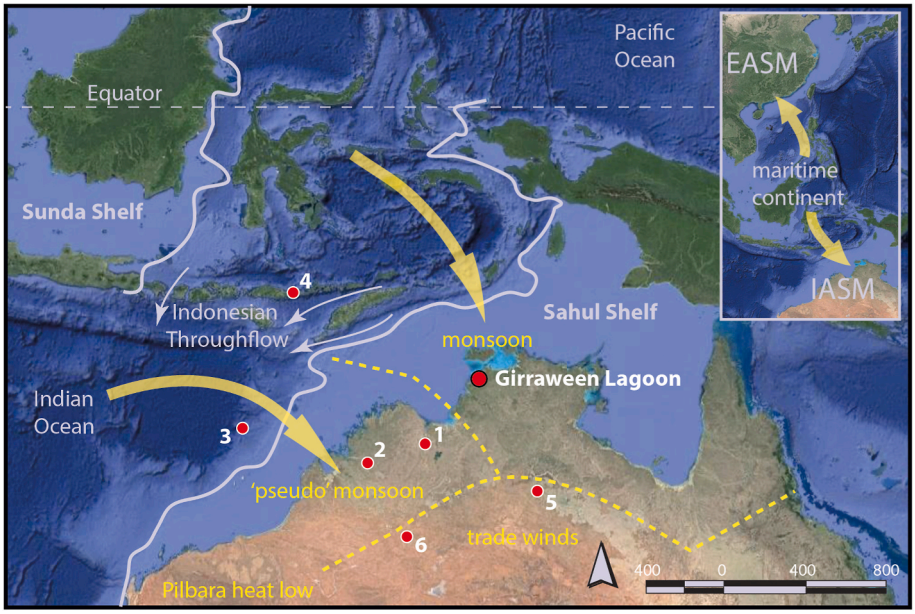

Fig. 1. Location of Girraween Lagoon in monsoonal north Australia. Also shown are the Sunda and Sahul continental shelves, with areas landward exposed at times of lower sea level, and the major pathways for water and heat transport between the Pacific and Indian Oceans via the Indonesian throughflow. Approximate boundaries of the true and 'pseudo' monsoon domains and directions of wet season airflow are in yellow (Suppiah, 1992). Insert shows the approximate dominant flows of the east Asian summer monsoon (EASM) and the Indo-Australian summer monsoon (IASM). Additional locations mentioned in the text are: 1 and 2: speleothem stable isotope records from KNI-51 and Ballgown Cave, respectively (Denniston et al., 2017); 3: marine core geochemical record of runoff and dust flux (Zhang et al., 2020; Pei et al., 2021; Sarim et al., 2023); 4: speleothem isotope record from Flores (Scroxton et al., 2022); 5 and 6: Woods and Gregory 'megalakes', respectively (Bowler et al., 1998, 2001; Fitzsimmons et al., 2012). Base image data: Google © 2023 Maxar Technologies. (For interpretation of the references to colour in this figure legend, the reader is referred to the Web version of this article.)

the drivers of megalake-filling events has centred on the relative importance of sea level, sea surface temperatures, and Northern Hemisphere 'push' *versus* Southern Hemisphere 'pull' of monsoonal rain into the continental interior, as well as the role of vegetation feedbacks in augmenting moisture transfer inland (Wyrwoll and Valdes, 2003; Liu et al., 2004; Miller et al., 2005; Pitman and Hesse, 2007; Marshall and Lynch, 2008; Wyrwoll et al., 2007, 2012).

Here we present multiple, absolute-dated proxy records of sedimentological, hydroclimatic, and vegetation change over the last 150 kyr from a sediment core obtained from the core monsoon region of northern Australia, the Girraween Lagoon (Fig. 1). This record enables an assessment of the timing of variation in monsoon strength in the Indo-Australian summer monsoon domain that can be compared with records of east Asian summer monsoon strength and tropical hydroclimate. Together, this enables an assessment of the drivers of variability in the Indo-Australian summer monsoon.

2. Materials and methods

2.1. Girraween Lagoon in monsoonal north Australia

Girraween Lagoon (12° 31′ 3.6″S, 131° 04′ 50.7″E; 25 m above sea level; Fig. 1) is a perennial waterbody currently 0.45 km^2 in area and 4.5 m in depth formed from a sinkhole collapse within a small 0.92-km^2 catchment (Rowe et al., 2019). The lagoon is in the core monsoon region of northern Australia, toward the southern margin of influence of the Indo-Australian summer monsoon. Since its formation, the lagoon has contained permanent water, and has therefore archived a rare, high-quality record of vegetation and climate change in the strongly seasonal Australian tropics (Rowe et al., 2019; Bird et al., 2024). Most (90 %) of the ~1700 mm annual rainfall is delivered in the wet season between November and April, currently supporting a mesic savanna that has developed over the course of the Holocene (Rowe et al., 2019).

A 19.4-m core was collected from the lagoon using a floating platform with hydraulic corer (Rowe et al., 2019). The record is composed of organic-rich sediments alternating with organic-poor clays (Fig. S1 and Table S1). An age-depth model for the record is provided by 12 radiocarbon and 24 optically stimulated luminescence ages, as detailed in Bird et al. (2024), with the age model reproduced in Fig. S1. Methods associated with development of the chronology for the Girraween record, determination of the variation in distance to the coast of the site over time, as well as the total organic carbon and pollen records, have been described previously (Bird et al., 2024).

2.2. Compound specific isotope analysis of n-alkanes

We extracted aliquots of 160 freeze-dried sediment samples from the length of the core of 10–50 g at 5–20 cm intervals depending on total organic carbon content. These were taken separately from samples used for the analysis of total organic carbon and pollen; hence, they are not always from the same depth interval. We placed the samples in dichloromethane:methanol (9:1) at 100 °C for 15 min in a MARS 6 microwave digestion system. We transferred the resulting total lipid extract into a 50-ml glass tube and evaporated to dryness under nitrogen, followed by transfer in hexane to a 4-ml glass vial. We separated alkanes using solid-phase extraction on a Restek 12 position solid-phase extraction vacuum SPE manifold using 6-ml Chroma bond SPE glass columns (Macherey-Nagel) filled with 1.5 g of silica gel (0.040- to 0.063-mm mesh size). We eluted the solvents and samples via stainless steel connectors and valves (Macherey-Nagel) to avoid plastic contamination. Once we cleaned the columns with n-hexane, dichloromethane, and acetone, we transferred each total lipid extract onto the column in hexane and eluted the alkanes with a further 10 ml n-hexane. Next, we added 10 μg 5a-androstane (Sigma-Aldrich) as an internal standard.

Most samples had multiple additional compounds that interfered with the measurements of the n-alkanes. We removed sulphur by loading the samples onto standard long-stem glass pipettes, half-filled with activated copper powder <425 μm (Sigma-Aldrich with a purity of 99.5 %). We activated the copper by washing with 6 ml of HCl and then rinsing with 10 ml Milli-Q water, followed by 6 ml acetone and 6 ml dichloromethane. We dissolved the samples in dichloromethane, transferred onto the copper pipette column, and rinsed five times with dichloromethane.

We removed alkenes from the samples with silver nitrate $AgNO_3$ on silica gel (Sigma-Aldrich). We activated $AgNO_3$ in an oven at 105 °C for 1 h, packed into long stem glass pipettes ¾ full, and kept out of direct UV light. After cleaning the packed column with acetone, dichloromethane, and n-hexane, we dissolved the samples, transferred them in *n*-hexane onto the $AgNO_3$ column and eluted them five times with *n*-hexane.

We removed branched alkanes from the samples using urea adduction. First, we transferred the sample (dissolved in n-hexane) into an 8-ml screw-top vial and evaporated it until dry with nitrogen. Then, we added three solutions to the vial: (*i*) 300 μl 10 % urea solution (Ultra-Pure Urea >98 %; Thermo-Fischer Scientific), (*ii*) 300 μl acetone, and (*iii*) 300 μl pentane (99 %; Scharlau). We then capped the vials, homogenised them with a vortex mixer, and placed into a freezer for 30 min, followed by evaporation to dryness under N_2. The urea crystallised as a precipitate with *n*-alkanes taken into channels in the urea structure while excluding branched alkanes. We rinsed the extracts with 1 ml n-hexane, leaving behind the clean urea crystals containing the *n*-alkanes. We repeated this procedure twice more, then added 500 μl ultraclean HPLC Plus grade water (Sigma-Aldrich), 500 μl methanol, and 1.5 ml *n*-hexane to dissolve the crystals, with the vial contents again homogenised by vortex mixer. We allowed the immiscible *n*-hexane (containing the *n*-alkanes) to separate above the water and methanol and then transferred them into another 8-ml vial. We repeated this step thrice. Once completed, we repeated the entire process 4 to 5 more times to eliminate all branched alkanes.

We identified and quantified the *n*-alkanes using a Shimadzu QP2010 gas chromatography-mass spectrometer GC-MS equipped with a mass-selective detector and a flame-ionisation detector coupled via an electronic split interface. We quantified through reference to the peak area of the internal standard 5a-androstane. We injected an aliquot of 1-μl sample into the GC-MS for each analysis. In addition, the GC-MS enabled confirmation of the elimination of impurities.

We determined the stable hydrogen isotope composition (δ^2H) and stable carbon isotope composition ($\delta^{13}C$) of the purified *n*-alkane samples in triplicate using a Trace 1310 gas chromatograph coupled to a Thermo-Scientific Delta V Plus isotope ratio mass spectrometer. The mass spectrometer measured the stable isotope composition of each compound (all n-alkanes present) in each sample. We converted the raw δ^2H to the isotopic water Vienna standard mean ocean water (VSMOW) scale through measurement of a standard containing n-alkanes of known stable isotope composition (Mix A4; Arndt Schimmelmann, Indiana University). We calibrated $\delta^{13}C$ with standards (Eicosane; Sigma-Aldrich, Androstane; Sigma-Aldrich, Docosane; Sigma-Aldrich, and Squalane; Alfa Aesar) to the international Vienna Pee Dee belemnite (VPDB) reference standard for carbon isotopes. Triplicate analysis enabled calculation of the uncertainty of each measurement of each *n*-alkane in each sample.

We used the mean of the abundant *n*-C_{27}, *n*-C_{29}, and *n*-C_{31} alkanes to represent the δ^2H and $\delta^{13}C$ of terrestrial plants (Hadeen et al., 2025). We applied a mass balance approach to calculate the equivalent δ^2H of plant available moisture (δ^2H_{pam}), involving correction for the differing hydrogen isotope fractionation associated with C_3 and C_4 photosynthesis, and for the effect of change in ocean δ^2H resulting from changes in the size of continental ice caps over the last glacial-interglacial cycle (Konecky et al., 2016). The average deviation from the mean of δ^2H_{pam} calculated in this way was ±6 ‰. The raw δ^2H values used for these calculations are available in Supplementary Table 1 and the $\delta^{13}C$ of the same *n*-C_{27}, *n*-C_{29}, and *n*-C_{31} alkanes are available in Hadeen et al. (2025).

2.3. Analysis

We applied a resampling approach for the correlations among proxies to take both age and value uncertainty into account. For each proxy, we drew 1000 random deviates of age using the *rtruncnorm* function in the rtruncnorm library (Mersmann et al., 2023) in the R programming language[88] and the mean and standard deviation of age (truncating to the interval 0 to ∞), and a random Normal deviate of the proxy value using the *rnorm* function. For each resampled time series, we then standardised the ages to the 150 ka ago to present period in 500-year intervals using the *approx* function and then scaled and centred the proxy values using the *scale* function.

To reduce the potential impact of temporal autocorrelation on the pairwise correlation between proxies, we applied two approaches. First, we resampled each proxy in the age-standardised and scaled pair without replacement but ensuring non-sequential values in each resample. We then applied a standard linear model using the *lm* function to each resampled pairwise combination and calculated the adjusted R^2 and type I error estimate (p_{rand}) for each pairwise model, calculating the 95 % confidence interval for both using the *quantile* function in R after 1000 iterations.

To test the association between Heinrich events and record time series, we compared the percentage of dryland tree and shrub pollen in the total dryland pollen sum *(%tree)* to the onset and termination of Heinrich events 0 to 12. Given that we do not expect immediate tree-growth responses to the change in climate conditions precipitated by Heinrich events, we asked whether there was empirical evidence to support the hypothesis that *%tree* was on average higher during Heinrich events than equivalent sampling windows either side of each Heinrich event. For this comparison, we developed a resampling approach where we incorporated three separate sources of uncertainty into the analysis (*i*) uncertainty in the age (absolute date) of the pollen counts for *%tree*, (*ii*) uncertainty in *%tree* based on the number of pollen grains sampled; and (*iii*) uncertainty in the onset of Heinrich events. We then generated 2000 random normal deviates of each dated *%tree* (i.e., 2000 replicates of 237 dated *%tree* values = 474,000 *%tree* values in total). Next, we resampled the onset of Heinrich events assuming uncertainties in the ages ranging from 0 to 2.5 %. For example, an uncertainty of 1 % for the onset of Heinrich 8 at 88.0 ka ago would give an onset range of 87.18 ka ago to 88.88 ka ago. In fact, there is some evidence that the true uncertainties can be at least 1 % of onset ages based on direct comparison between terrestrial and marine indicators of Heinrich events offshore of the Amazon River (Jennerjahn et al., 2004). To the randomised onsets, we added the deterministic duration (e.g., for Heinrich 8, duration = 2.5 kyr) to give a range of Heinrich terminations. We then established two 'non-Heinrich' sampling windows either side of each resampled Heinrich event of the same duration as the Heinrich event itself. We corrected for any event overlaps (e.g., no Heinrich or non-Heinrich event could overlap in time with its nearest event neighbour) by taking the midpoint for any overlapping events. As we increased uncertainty in onset, the number of overlaps increased. We then took a random sample of 100 *%tree* replicates per event based on the resampled values, noting when they fell within Heinrich or non-Heinrich events, calculating the median *%tree* for each event, and repeated this procedure 100,000 times.

For each of those 100,000 iterations, we recorded when mean *%tree* was higher than at least one of the non-Heinrich sampling windows immediately adjacent to each Heinrich event. We compared the number of times this occurred in each iteration to the null model of generating the same response at random (i.e., a binomial-resampled value based on the number of Heinrich events in each iteration). Here, we calculated the probability that the instances when *%tree* in Heinrich events exceeded those in non-Heinrich events could be generated at random under the null model (when this probability is low, it indicates statistical support for the hypothesis that *%tree* was higher on average during Heinrich compared to non-Heinrich events). All code and data necessary to repeat the analyses are available at https://doi.org/10.5281/zenodo.10791249.

3. Results and discussion

3.1. Proxy indicators from Girraween lagoon

The percentage of dryland tree (and shrub) pollen in the total dryland pollen sum (*%tree*) is a sensitive indicator of past changes in hydroclimate (Bird et al., 2024). The major determinant of savanna vegetation structure is moisture availability, determined mainly by rainfall and evaporation, but modulated by intraseasonal/interannual rainfall variability and feedbacks on tree recruitment associated with fire return interval/intensity and herbivory (Hutley et al., 2001, 2011; Xu et al., 2018; Gosling et al., 2022; Williamson et al., 2024). Across the broader study region, there is a strong relationship between tree cover and mean annual precipitation (Bird et al., 2019). Savanna vegetation can respond rapidly to changes in climate (Oliveras and Malhi, 2016; Xu et al., 2023), particularly in regions of high rainfall variability such as northern Australia (Poulter et al., 2014). Tree pollen as a percentage of total terrestrial pollen in the record ranges from <5 % to >95 % (Fig. 2b and S2), indicating large shifts on centennial timescales from open grassy savanna to functionally closed forest. This in turn indicates large, rapid changes in hydroclimate in the past.

The hydrogen isotope composition of terrestrially derived *n*-alkanes, converted to the equivalent hydrogen isotope composition of plant available moisture (δ^2H_{pam}; see Methods) provides information on changes in rainfall regime, likely associated with changes in monsoon intensity and changes in the distance of the site to the ocean. Controls on modern rainfall δ^2H are well-established from seven years of daily measurements of rainfall from a location 20 km from the lagoon (Zwart et al., 2018). More positive rainfall δ^2H values ($\gtrsim -40$ ‰) are associated with periods where shallow continental convection dominates and convection is forced by sea breezes. More negative rainfall δ^2H ($\lesssim -40$ ‰ and as low as −100 ‰) is associated with periods of intense rainfall when the monsoon trough is active and stratiform cloud area is large (Zwart et al., 2018).

On millennial timescales, δ^2H_{pam} will be partly determined by monsoon intensity. However, δ^2H_{pam} at this location is also modified by distance to the coastline because the shallow gradient offshore means that the coastline position receded up to 320 km during peak glacial periods (Fig. 2c), and there is a rapid decrease in precipitation inland from the modern coast (Hutley et al., 2001, 2011) that will also have existed in the past. This is particularly important for the interpretation of the Girraween record because evapotranspiration of previous precipitation contributes to the penetration of precipitation into the continental interior (Sharmila and Hendon, 2020). Evaporation moisture contributing to rainfall farther inland will result in a progressively higher δ^2H in subsequent precipitation farther inland, thereby diluting the primary 'monsoon' rainfall δ^2H. We note also that, δ^2H_{pam} can be influenced by changes in moisture-source region (Konecky et al., 2019). δ^2H_{pam} in the Girraween record ranges widely from −85 ‰ to +35 ‰, reflecting the sum of all the above sources of variability (Fig. 2b and Fig. S2).

Total organic carbon in the Girraween record is interpretable as a record of past lake level. Currently, the lake extends over 0.45 km^2 (doubling again in size during flood events), with the area $\lesssim$ 2.5 m deep (~70 % of the total area) suitable for colonisation by rooted macrophytes. At such times of high lake level there is therefore an excess of photosynthetic organic matter production over what can be respired. The Holocene sediments in the lake are carbon-rich for this reason, similar to previous intervals in the record with high (or indeed higher) total organic carbon (Fig. S1 and Table S1). At other times of low lake level, the sediments were entirely different — greenish to greyish clays with little organic matter. The transition between these sediment types tends to be abrupt in most cases because during dry phases the local water table decreased and the lagoon retreated into the steep-walled sinkhole itself. Lagoon surface area was reduced by 1–2 orders of

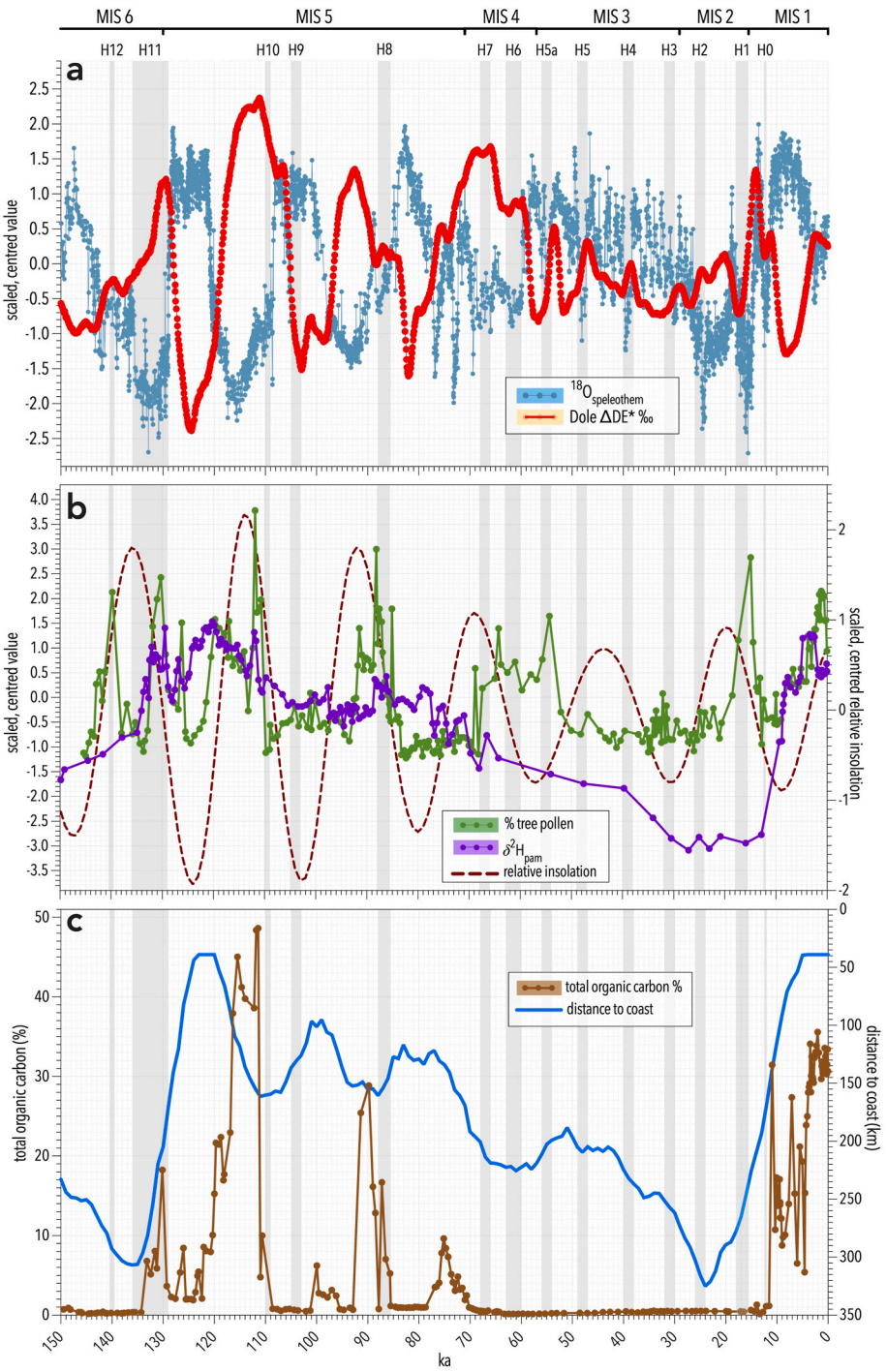

Fig. 2. (a) Composite east Asian summer monsoon speleothem oxygen isotope record (Cheng et al., 2016) and the Dole effect (ΔDE*) record (Huang et al., 2020). (b) δ^2H_{pam} (hydrogen isotope composition of plant available moisture) and *%tree* pollen of total dryland pollen records from Girraween Lagoon summer (January-February–March) insolation at 18 °S; all values are scaled and centred for correlation (see Methods, and extended data Figs. S2 and S3 for unscaled time series in original units with analytical errors). (c) Total organic carbon record from Girraween Lagoon and distance to coast (Bird et al., 2024). The timing of Heinrich events is indicated as grey shading and Marine Isotope Stage boundaries also shown, both from Lisieki and Stern (2016). The age of 140 ka for 'H12' in Lisieki and Stern (2016) is derived from the average age of two events centred on 135.5 ka and 144.3 ka (with no duration given for either event) identified by Channell et al. (2012), so 'H12' is likely of longer duration than shown above.

magnitude and there was limited shallow water area for carbon production by rooted macrophytes due to the deep water of the sinkhole. Photosynthetic production that was possible was mostly respired in the water column or surface sediment, hence the low total organic carbon in the sediments. Thus, total organic carbon exhibits a threshold 'on-off' response to changes in rainfall (Bird et al., 2024). Total organic carbon ranges from <0.5 % to >40 % (Fig. 2c), with periods of highest total organic carbon (≳ 20 %) occurring at times of high local insolation, when the coast was ≲ 200 km distant, in MIS 5 and 1.

3.2. *Comparison with other monsoon proxies*

Our proxy records can be compared with time series of (*i*) local wet season insolation (Fig. 2b), (*ii*) the Chinese speleothem oxygen isotope

compilation representing east Asian summer monsoon dynamics (Cheng et al., 2016) (Fig. 2a and S3), and (*iii*) ΔDE* — the modified Dole effect that mainly reflects the intensity of the low-latitude terrestrial hydrological cycle globally, where more negative ΔDE* values indicate intensification (Huang et al., 2020) (Fig. 2a and S3).

We acknowledge that these comparator records are more highly resolved than the Girraween records and are supported by more precise age models. Nevertheless, the multiproxy nature of the Girraween record (Fig. 2b and c) provides the opportunity for more nuanced interpretation of local hydroclimate dynamics than any single-proxy time series. The age model is reliable to within ~5 % of the mean with 95 % confidence for its entire length, and therefore sufficiently constrained to be able to examine correlations between the records.

To demonstrate that our age model is reliable at the older end of the range, we compare the average chain length of the *n*-alkanes from the Girraween record with the 115–150 ka marine *n*-alkane record of Huang et al. (2015) from the Timor Sea, 500 km northwest of our site (Fig. S4). There is no reason for the detail in the two records to match, because the marine record is more influenced by vegetation on the islands of Wallacea, while our record is influenced by local conditions in northern Australia. However, it is reasonable to expect that the major climate changes associated with the start of Termination II (~136 ka) should be visible in both records and the major change occurs within 2000 years of each other in both records.

Statistical comparison between our results and other time series indicates that there is some concordance between the major increases in monsoon intensity in the Girraween record at times of high local insolation centred on 115 ka, 92 ka, 75 ka, and in the Holocene when the coast was near (Fig. 2), but neither %*tree* nor δ^2H_{pam} in the Girraween record is correlated with insolation in its entirety (%*tree*: resampled R^2 = 0–0.18, p = 0.0012–0.8764, β = −0.01–0.46, ρ = −0.035–0.399; δ^2H_{pam}: resampled R^2 = 0–0.05, p = 0.0762–0.9853, β = −0.25–0.17, ρ = −0.220–0.192). There is also a strong anti-phase between the timing of maxima and minima in the Girraween proxies and the east Asian summer monsoon speleothem isotope record, although the changing distance to coast at Girraween decreases the evidence for correlation over the full time series (^{18}O speleothem–%*tree*: resampled R^2 = 0–0.16; p = 0.0028–0.9265; β = −0.06–0.42; ρ = −0.087–0.365; ^{18}O speleothem–δ^2H_{pam}: resampled R^2 = 0–0.07; p = 0.0407–0.9726; β = −0.21–0.27; ρ = −0.216–0.273; ΔDE*–%tree: resampled R^2 = 0–0.22; p = 0.0004–0.8611; β = 0.001–0.49; ρ = −0.019–0.450; ΔDE*–δ^2H_{pam}: resampled R^2 = 0–0.09; p = 0.0177–0.9692; β = −0.35–0.13; ρ = −0.321–0.131).

3.3. Cyclic and abrupt changes in monsoon hydroclimate over the last 150,000 years

All proxy records from Girraween Lagoon indicate large changes in local hydroclimate occurred over both multi-millennial and sub-millennial time scales. Coincident intervals of negative δ^2H_{pam}, high tree cover, and high total organic carbon unequivocally indicate periods of higher rainfall. Over the entire record, glacial stages MIS 2 and MIS 6 clearly represent periods of (usually) lower rainfall, while interglacial MIS 1 and (periodically) MIS 5 represent periods of highest rainfall, generally consistent with the available body of evidence for northern Australia (Bowler et al., 1998, 2001; Fitzsimmons et al., 2012; Cohen et al., 2022).

Two wet events are suggested by increases in the %*tree* record that occur in MIS 6. The earliest at 140 ka is coincident with Heinrich 12. The coast was ~300 km distant at this time, and the change in rainfall was not large enough to cause a change is observed in δ^2H_{pam} or total organic carbon content. The second wet event is coincident with Heinrich 11 (Termination II; Fig. 2b) and despite the coast being >150 km distant at that time, it is recorded in all three proxies (Fig. 2c).

A relative reduction in monsoon activity during MIS 5e is indicated by a decrease in total organic carbon and tree cover despite the coast being adjacent to the site at that time. A regionally drier MIS 5e, even though the coast was adjacent to the site, is consistent with model predictions due to low local insolation at that time (Nilsson-Kerr et al., 2021; Yeung et al., 2021).

The most intense monsoon event in the record is centred on the local summer insolation maximum at 115 ka (MIS 5d), culminating in a brief period at 112 ka of low δ^2H_{pam} and the development of functionally closed forest (>95 % tree pollen), despite the coast being 150 km distant. This timing, during a period of high insolation, is consistent with the existence of 'megalakes' south of the site (Bowler et al., 2001; Fitzsimmons et al., 2012; Cohen et al., 2022). Wyrwoll and Valdes (2003) modelled an increase to 130 % of modern rainfall across north-western Australia at 115 ka, the time of maximum local insolation over the full length of the record, despite sea level being lower than present and hence the coast being ~ 100 km farther away than present.

Another peak in monsoon activity expressed as rapid changes in %*tree*, δ^2H_{pam}, and total organic carbon (Fig. 2b) is broadly coincident with another peak in local insolation centred at 90 ka. This event differed from earlier wet events in being accompanied by a consistent increase of ~10 ‰ in δ^2H_{pam} from 97 ka to 88 ka, suggesting a change in moisture-source area involving a shift to the east of the monsoon-'pseudo' monsoon boundary, a possibility also supported by model predictions (Wyrwoll et al., 2012). The timing of this wet interval is also consistent with 'megalake' filling to the south (Bowler et al., 2001; Cohen et al., 2022).

Increases in total organic carbon, %*tree*, and a small but abrupt decrease δ^2H_{pam} between 88 ka and 85 ka occurred at a time equivalent to Heinrich 8. It is possible that an additional increase in total organic carbon in line with increasing local summer insolation toward 69 ka was truncated because of the rapid increase in distance to the coast to beyond 200 km (Fig. 2c) that attended rapid sea level fall at the beginning of MIS 4 through to MIS 2. MIS 4 is characterised in the regional literature as a return to 'full glacial' conditions (Schaefer et al., 2015; De Deckker et al., 2019). Nevertheless, wet events are evident in increased tree cover within chronological uncertainty of Heinrich events 7, 6, and 5a (Fig. 2b) between 65 ka and 45 ka, a timing that overlaps with 'megalake' filling events farther south (Bowler et al., 1998; Veth et al., 2009; Cohen et al., 2022).

δ^2H_{pam} exhibits a progressive increase from the beginning of MIS 4 that continues into the Last Glacial Maximum. During this time the coast was always >200 km (and up to 320 km) distant, total organic carbon was uniformly low, and this resulted in a poorly resolved δ^2H_{pam} record due to adjacent samples being combined to provide a large enough sample for analysis. In addition, rainfall reaching the site as the coastline receded would be progressively modified to higher δ^2H by an evaporated, recycled soil moisture component (Sharmila and Hendon, 2020).

As a result of the progressive retreat of the coastline, the δ^2H_{pam} record does not indicate any periods of increased monsoon activity during that time, even when tree cover increased and therefore moisture availability increased or seasonality decreased, for example during Heinrichs 3 and 2. δ^2H_{pam} over this interval suggests overall decreasing, increasingly evaporated, local moisture availability into the Last Glacial Maximum. Annual rainfall during maximum sea-level depression (~320 km) accompanying the Last Glacial Maximum, a time of low local insolation, has been estimated from the pollen spectra at < 1000 mm (Rowe et al., 2021). This is equivalent to a ≥43 % decrease compared to modern rainfall at the site.

Heinrich Event 1 (Termination I) is characterised by a large, rapid increase in tree cover (briefly to 78 %) between 17.5 ka and 14.5 ka. This suggests increased rainfall, and/or decreased seasonality at the time, but any increase did not result in the lagoon filling to the point where total organic carbon increased. Only two δ^2H_{pam} estimates are available at that time due to low total organic carbon that required the bulking of adjacent samples encompassing almost 10 kyr; hence, no monsoon isotope signal can be discerned. However, that Termination 1 was accompanied by a wet event in the region is supported by speleothem

records to the west (Denniston et al., 2017) and Flores to the north (Scroxton et al., 2022) of the site (Fig. S6). Wyrwoll and Miller (2001) also identified monsoon 'reactivation' around the time of Termination 1 with dated material indicating wetter conditions ranging in age from 15.6 ka to 13.1 ka. The lake-level threshold leading to high total organic carbon was not exceeded until 11 ka at Girraween Lagoon, δ^2H_{pam} returned to the range observed in MIS 5 and tree cover increased progressively during the Holocene indicating active monsoon conditions.

3.4. A relationship between Heinrich events and north Australian monsoon intensification?

If local insolation, modulated by distance to the coast, were the main drivers of hydroclimate change over the length of the record, we would expect to see a correlation between these drivers and all the Girraween proxies of hydroclimate. While there is some concordance between the major increases in monsoon intensity in the Girraween record at times of high local insolation when the coast was near (see results for statistics), the δ^2H_{pam} and *%tree* records longer-term trends in both are interspersed by often large, relatively short-term perturbations to higher monsoon intensity occurring over ~1 to < 10 kyr (Fig. 2). In the most extreme case, *%tree* changes from 20 % to 95 % over 3 kyr, and back to 5 % over an additional 3 kyr, in the six samples between 110 and 116 ka (this relative change in measured values is independent of uncertainty in the absolute age). Over the same interval, δ^2H_{pam} decreased from −55 ‰ to −80 ‰, and then increased to −45 ‰ (Fig. S2). Likewise, large changes in both *%tree* and δ^2H_{pam} between 138 and 128 ka during Heinrich 11 (Termination II), are evident in a coherent increase then decrease over 8 samples representing ~ 10 kyr, at a time when the coast was >200 km distant but approaching, and insolation was decreasing. Other instances of rapid change occur throughout the record, that appear mostly independent of either insolation or distance to coast.

There is concordance between these rapid, short-term increases in monsoon intensity in the Girraween record that coincide with ($n = 7$), or are within, chronological uncertainty of ($n = 3$), Heinrich events including Termination II (Heinrich event 11), and Termination I (Heinrich event 1), noting that the manifestation of perturbations associated with Heinrich events in the North Atlantic might involve a lag to other parts of the world (e.g., Jennerjahn et al., 2004). A randomisation of the onset of Heinrich events *versus* the *%tree* record (that incorporates uncertainties in both the age model and pollen counts; see Methods) reveals a non-random association (type 1 error <0.03 to < 0.05) for uncertainties in Heinrich onset timing from 0 to 1.8 % (see Methods and Fig. S5). This indicates strong evidence for an association between the timing of Heinrich Events and the timing of changes in the pollen record indicating monsoon intensification at Girraween Lagoon. There are also clear, negative excursions in the δ^2H_{pam} series during Heinrich events where the record is sufficiently resolved and the coast is < 100 km distant. Overall, the δ^2H_{pam} association with Heinrich events is weaker ($p_{rand} = 0.1506$), the relationship in parts of the record being confounded by decreased sensitivity associated with a long distance to the coast and low sample resolution through MIS 6 and most of MIS 4 to MIS 2.

The strong anti-phase between the timing of maxima and minima in the Girraween proxies and the east Asian summer monsoon speleothem isotope record suggests strong, cross-equatorial coupling resulting in an anti-phase, precession-driven relationship. Thus, peaks in monsoon activity at 140 ka, 126 ka, 106 ka, and 80 ka in the east Asian summer monsoon domain correspond to dry intervals in the Girraween record — wet intervals in the Girraween record at 135 ka, 115 ka, and 92 ka are dry periods in the east Asian summer monsoon domain. From MIS 4, the coast was always >200 km from Girraween until the end of MIS 2 and the Girraween record becomes less strongly correlated to the east Asian summer monsoon record.

There are few other regional terrestrial records to compare, but wet events considered to be most likely attributed to Heinrich events 5a, 5, 2, 1, and 0 are recorded in a Flores speleothem isotope record (Scroxton et al., 2022) 1000 km northwest of Girraween Lagoon also in the Indo-Australian summer monsoon domain (Fig. S6). A discontinuous composite speleothem record (Denniston et al., 2017), 1000 km southwest of the Girraween site, indicates wetter periods coinciding with Heinrich event 4, (no data for 3), 2, 1, and 0 (Fig. S6).

In combination with the Girraween record (that records no obvious signal for Heinrich events 9, 4 or 0), the data available from the Girraween site and broader Indo-Australian summer monsoon region suggest that all Heinrich events except Heinrich event 9 resulted in detectable change in monsoon intensity, generally toward intensification. In contrast to their expression in northern Australia, Heinrich events coincide with weak monsoon intervals (Cheng et al., 2009, 2016) in the east Asian summer monsoon domain (Fig. 2a).

The *%tree* record appears the most consistently sensitive to changes in moisture balance (amount and/or seasonality), even when the coast was far from the site, but the δ^2H_{pam} record also indicates increased intensity of monsoonal rainfall coinciding with Termination II (Heinrich event 11), Heinrich events 10, 8, and possibly 6. After Heinrich event 6, the long distance to the coast, and the low sample numbers due to low total organic carbon rendered the δ^2H_{pam} record insensitive to short-term change until the Holocene. With the exception of Termination II (Heinrich event 11), the gross changes recorded by the total organic carbon record appear more driven by long-term changes in insolation, although these generally wet intervals encompass Heinrich events 10, 8, and possibly 0.

The wet periods inferred from the Girraween record correlated to Heinrich events coincide closely in time with major or minor peaks in the ΔDE* record occurring at, or within, chronological uncertainty of all Heinrich events except 9, 1, and 0; however, the full ΔDE* time series is not associated with the position of Heinrich events ($p_{rand} = 0.3436$).

Terrestrial records from elsewhere in the Southern Hemisphere monsoon domain are sparse but suggest that monsoon intensification across the low latitudes of the Southern Hemisphere during Heinrich events might have been a widespread phenomenon. A record of episodic speleothem and travertine formation from semi-arid northeastern Brazil indicates brief wet events coinciding with Heinrich events 11 (Termination II), 10, 6, 5, 4 and 1 (Termination 1) (Wang et al., 2004), while a 50 kyr salt lake record from the Bolivian altiplano recorded Heinrich events 2, 1, and 0 (Baker et al., 2001). Cheng et al. (2013) identified speleothem isotope excursions associated with Heinrich events 5 to 1. Placzek et al. (2013) identified wet intervals associated with Heinrich events 5, 2, 1 and 0 on the Pacific Ocean side of the Bolivian altiplano. Modelling has also suggested that freshwater hosing associated with Heinrich events leads to southward displacement of the inter-tropical convergence zone because of increased sea-surface temperatures in the Southern Hemisphere generally (Singarayer et al., 2017).

4. Conclusions

4.1. Link between Indo-Australian summer monsoon and Heinrich events?

We have demonstrated that over the last 150 kyr, monsoon rainfall at the southern limit of the Indo-Australian summer monsoon domain in northern Australia is strongly anti-phased with east Asian summer monsoon rainfall, particularly during interglacial periods. This is unsurprising given the cross-equatorial coupling of the two monsoon systems. We have also identified that the large changes in coastal position that occur in response to seal level change on a wide flat coastal shelf reduced rainfall on what is now the Australian continent, regardless of changes in the intensity of the monsoon. This would have diverse implications for the interpretation of all long environmental records in northern Australia. Indeed, the drying of Kati Thandi-Lake Eyre after 43 ka (Cohen et al., 2022) might be partly a consequence of the retreat of the northern Australian coastline from MIS3 into the Last Glacial Maximum.

We have demonstrated evidence for an association between monsoon intensity (and/or seasonality of rainfall) in northern Australia, inferred from rapid, short-term increases in tree cover and decreases in some cases in δ^2H_{pam}, and the timing of Heinrich events. Our interpretation is supported by the observations that (*i*) short, dry periods evident in the east Asian summer monsoon speleothem record have been securely linked to Heinrich events (Cheng et al., 2009, 2016), (ii) the Indo-Australian and east Asian summer monsoons are known to be coupled in anti-phase (Li and Li, 2014), (*iii*) modelling suggests a southward shift in the Southern Hemisphere monsoon globally in response to Heinrich event forcing (Singarayer et al., 2017), and (*iv*) that other Southern Hemisphere records also suggest Heinrich events result in wetter conditions (Baker et al., 2001; Wang et al., 2004; Cheng et al., 2013; Placzek et al., 2013). Indeed, it is difficult to envisage another driver that could explain such rapid and large, but short-term changes in vegetation, let alone a driver that coincides so consistently with the timing of Heinrich events.

4.2. Implications of a link between the Indo-Australian summer monsoon and Heinrich events

Changes in inter-hemispheric thermal contrast driven by sea surface temperature and influenced by different land-ocean areas in the two hemispheres contribute to north-south asymmetry in tropical rainfall over multidecadal timescales (Sun et al., 2013; Xue et al., 2022). It is possible that differences in thermal contrast between the hemispheres on glacial-interglacial time frames also create an asymmetry in rainfall response between the east Asian and Indo-Australian summer monsoons, and indeed between the Northern and Southern Hemispheres more generally (Singarayer et al., 2017; Xue et al., 2022).

If Heinrich events in the past were the catalyst for the major abrupt, millennial-scale increases in monsoon intensity identified in the Girraween Lagoon and other regional records, then a link possibly exists between the Indo-Australian summer monsoon and the strength of the Atlantic meridional overturning circulation, decreases thought to trigger Heinrich events (Böhm et al., 2015). Decreased strength of the Atlantic meridional overturning circulation leads to reduced oceanic heat transport from the Southern to Northern Hemisphere (Shackleton et al., 2020; Max et al., 2022).

Modelling based on modern boundary conditions predicts a shutdown of the Atlantic meridional overturning circulation has diverse implications across the tropics. These include Southern Hemisphere warming and development of an anomalous, inter-hemispheric temperature gradient (Orihuela-Pinto et al., 2022), as well as southward displacement of the intertropical convergence zone and a weakened east Asian summer monsoon (Zhang and Delworth, 2005). Slowing of the Atlantic meridional overturning circulation during Termination II is also predicted to have had similar outcomes (Guarino et al., 2023).

Current weakening of the Atlantic meridional overturning circulation was probably initiated in the 20th Century (Dima et al., 2021; Pontes and Menviel, 2024) and has been measured over the last 40 years (Piecuch and Beal, 2023). This weakening is projected to continue because of anthropogenic climate change (Dima et al., 2021). Indeed, recent work has suggested that the Atlantic meridional overturning circulation is on track to pass a tipping point, two results of which will be drying in Southeast Asia, and an increase in rainfall across much of the Southern Hemisphere tropics, including Australia (van Westen et al., 2024).

A trend to decreasing rainfall in the east Asian summer monsoon identified in speleothem isotope records has been underway since the late 19th Century (Zhao et al., 2023), and is evident in rainfall records (Guo et al., 2020) since the 1960s. A trend to increasing Indo-Australian summer monsoon rainfall in north-western Australia has been underway for the last century (Heidemann et al., 2023), accelerating since the 1950s. The data from our study suggest that further weakening of the Atlantic meridional overturning circulation could reinforce these trends in the future.

Code availability

All code available at: https://doi.org/10.5281/zenodo.10791249.

Contributions

MIB, CMW, and CR designed the study. MIB, CR, CMW, MB, RC, XH, ZJ, and CZ did field sampling and laboratory analyses, FS and CJAB did the statistical analyses. All authors contributed to the interpretation. MIB wrote the initial manuscript, and all authors contributed to the final form of the manuscript.

Ethics declarations

.

Declaration of competing interest

The authors declare that they have no known competing financial interests or personal relationships that could have appeared to influence the work reported in this paper.

Acknowledgements

Funded by the Australian Research Council Centre of Excellence for Australian Biodiversity and Heritage through CE170100015 to MIB, ZJ, and CJAB and an Australian Research Council Laureate Fellowship to MIB (FL140100044). We thank Larrakia Traditional Owners for permission to do this research on their traditional lands.

Appendix A. Supplementary data

Supplementary data to this article can be found online at https://doi.org/10.1016/j.quascirev.2025.109504.

Data availability

All data and/or code is contained within the submission.

References

An, Z., Wu, G., Li, J., Sun, Y., Liu, Y., Zhou, W., Cai, Y., Duan, A., Li, L., Mao, J., Cheng, H., Shi, Z., Tan, L., Yan, H., Ao, H., Chang, H., Feng, J., 2015. Global monsoon dynamics and climate change. Annu. Rev. Earth Planet Sci. 43, 29–77.

Baker, P.A., Rigsby, C.A., Seltzer, G.O., Fritz, S.C., Lowenstein, T.K., Bacher, N.P., Veliz, C., 2001. Tropical climate changes at millennial and orbital timescales on the Bolivian Altiplano. Nature 409, 698–701.

Bird, M.I., Brand, M., Diefendorf, A.F., Haig, J.L., Hutley, L.B., Levchenko, V., Ridd, P.V., Rowe, C., Whinney, J., Wurster, C.M., Zwart, C., 2019. Identifying the 'savanna' signature in lacustrine sediments in northern Australia. Quat. Sci. Rev. 203, 233–247.

Bird, M.I., Brand, M., Comley, R., Fu, X., Hadeen, X., Jacobs, Z., Rowe, C., Wurster, C.M., Zwart, C., Bradshaw, C.J.A., 2024. Late Pleistocene emergence of an Anthropogenic fire regime in Australia's tropical savanna. Nat. Geosci. 17, 233–240.

Böhm, E., Lippold, J., Gutjahr, M., Frank, M., Blaser, P., Antz, B., Fohlmeister, J., Frank, N., Andersen, M.B., Deininger, M., 2015. Strong and deep Atlantic meridional overturning circulation during the last glacial cycle. Nature 517, 73–76.

Bowler, J.M., Duller, G.A.T., Perret, N., Prescott, J.R., Wyrwoll, K.H., 1998. Hydrologic changes in monsoonal climates of the last glacial cycle: stratigraphy and luminescence dating of Lake Woods, NT, Australia. Palaeoclimates 3, 179–207.

Bowler, J.M., Wyrwoll, K.H., Lu, Y., 2001. Variations of the northwest Australian summer monsoon over the last 300,000 years: the paleohydrological record of the Gregory (Mulan) Lakes System. Quat. Int. 83, 63–80.

Channell, J.E., Hodell, D.A., Romero, O., Hillaire-Marcel, C., de Vernal, A., Stoner, J.S., Mazaud, A., Röhl, U., 2012. A 750-kyr detrital-layer stratigraphy for the North Atlantic (IODP sites U1302–U1303, Orphan Knoll, Labrador Sea). Earth Planet Sci. Lett. 317, 218–230.

Chen, C., Huang, K., Zheng, Z., Zong, Y., Kershaw, P., Yang, S., Tian, L., Man, M., Li, S.H., Brodie, C., Wang, N., 2023. Savanna/rainforest dynamics and hydroclimate changes in northern boundary of tropical Asia over the past 150 kyrs. Global Planet. Change 228, 104204.

Cheng, H., Sinha, A., Cruz, F.W., Wang, X., Edwards, R.L., d'Horta, F.M., Ribas, C.C., Vuille, M., Stott, L.D., Auler, A.S., 2013. Climate change patterns in Amazonia and biodiversity. Nat. Commun. 4, 1411.
Cheng, H., Edwards, R.L., Broecker, W.S., Denton, G.H., Kong, X., Wang, Y., Zhang, R., Wang, X., 2009. Ice age terminations. Science 326, 248–252.
Cheng, H., Edwards, R.L., Sinha, A., Spötl, C., Yi, L., Chen, S., Kelly, M., Kathayat, G., Wang, X., Li, X., Kong, X., 2016. The Asian monsoon over the past 640,000 years and ice age terminations. Nature 534, 640–646.
Cohen, T.J., Arnold, L.J., Gázquez, F., May, J.H., Marx, S.K., Jankowski, N.R., Chivas, A. R., Garćia, A., Cadd, H., Parker, A.G., Jansen, J.D., 2022. Late quaternary climate change in Australia's arid interior: evidence from Kati Thanda–Lake Eyre. Quat. Sci. Rev. 292, 107635.
Cook, E.R., Anchukaitis, K.J., Buckley, B.M., D'Arrigo, R.D., Jacoby, G.C., Wright, W.E., 2010. Asian monsoon failure and megadrought during the last millennium. Science 328, 486–489.
De Deckker, P., Arnold, L.J., van der Kaars, S., Bayon, G., Stuut, J.B.W., Perner, K., dos Santos, R.L., Uemura, R., Demuro, M., 2019. Marine Isotope Stage 4 in Australasia: a full glacial culminating 65,000 years ago–global connections and implications for human dispersal. Quat. Sci. Rev. 204, 187–207.
Deininger, M., McDermott, F., Cruz, F.W., Bernal, J.P., Mudelsee, M., Vonhof, H., Millo, C., Spötl, C., Treble, P.C., Pickering, R., Scholz, D., 2020. Inter-hemispheric synchroneity of Holocene precipitation anomalies controlled by Earth's latitudinal insolation gradients. Nat. Commun. 11, 5447.
Denniston, R.F., Asmerom, Y., Polyak, V.J., Wanamaker Jr, A.D., Ummenhofer, C.C., Humphreys, W.F., Cugley, J., Woods, D., Lucker, S., 2017. Decoupling of monsoon activity across the northern and southern Indo-Pacific during the Late Glacial. Quat. Sci. Rev. 176, 101–105.
Dima, M., Nichita, D.R., Lohmann, G., Ionita, M., Voiculescu, M., 2021. Early-onset of Atlantic Meridional Overturning Circulation weakening in response to atmospheric CO2 concentration. NPJ Climate and Atmospheric Science 4, 27.
Eroglu, D., McRobie, F.H., Ozken, I., Stemler, T., Wyrwoll, K.H., Breitenbach, S.F., Marwan, N., Kurths, J., 2016. See–saw relationship of the Holocene East Asian–Australian summer monsoon. Nat. Commun. 7, 12929.
Fitzsimmons, K.E., Miller, G.H., Spooner, N.A., Magee, J.W., 2012. Aridity in the monsoon zone as indicated by desert dune formation in the Gregory Lakes basin, northwestern Australia. Aust. J. Earth Sci. 59, 469–478.
Gallagher, S.J., Korasidis, V.A., Auer, G., De Vleeschouwer, D., Groeneveld, J., Christensen, B., 2024. Cenozoic history of the Australian Monsoon. Prog. Earth Planet. Sci. 11, 60.
Gosling, W.D., Miller, C.S., Shanahan, T.M., Holden, P.B., Overpeck, J.T., van Langevelde, F., 2022. A stronger role for long-term moisture change than for CO_2 in determining tropical woody vegetation change. Science 376, 653–656.
Guarino, M.V., Sime, L.C., Diamond, R., Ridley, J., Schroeder, D., 2023. The coupled system response to 250 years of freshwater forcing: last Interglacial CMIP6–PMIP4 HadGEM3 simulations. Clim. Past 19, 865–881.
Guo, B., Zhang, J., Meng, X., Xu, T., Song, Y., 2020. Long-term spatio-temporal precipitation variations in China with precipitation surface interpolated by ANUSPLIN. Sci. Rep. 10, 81.
Hadeen, X., Rowe, C., Brand, M., Comley, R., Das, S., Wurster, C.M., Zwart, C., Bird, M.I., 2025. Comparing pollen and *n*-alkane carbon isotope records in a tropical lacustrine environment. Quat. Sci. Rev. 351, 109204.
Heidemann, H., Cowan, T., Henley, B.J., Ribbe, J., Freund, M., Power, S., 2023. Variability and long-term change in Australian monsoon rainfall: a review. Wiley Interdisciplinary Reviews: Clim. Change 14, e823.
Huang, E., Tian, J., Liu, J., 2015. Dynamics of the Australian–Indonesian monsoon across Termination II: implications of molecular-biomarker reconstructions from the Timor Sea. Palaeogeogr. Palaeoclimatol. Palaeoecol. 423, 32–43.
Huang, E., Wang, P., Wang, Y., Yan, M., Tian, J., Li, S., Ma, W., 2020. Dole effect as a measurement of the low-latitude hydrological cycle over the past 800 ka. Sci. Adv. 6, eaba4823.
Hutley, L.B., O'Grady, A.P., Eamus, D., 2001. Monsoonal influences on evapotranspiration of savanna vegetation of northern Australia. Oecologia 126, 434–443.
Hutley, L.B., Beringer, J., Isaac, P.R., Hacker, J.M., Cernusak, L.A., 2011. A sub-continental scale living laboratory: spatial patterns of savanna vegetation over a rainfall gradient in northern Australia. Agric. For. Meteorol. 151, 1417–1428.
Jennerjahn, T.C., Ittekkot, V., Arz, H.W., Behling, H., Patzold, J., Wefer, G., 2004. Asynchronous terrestrial and marine signals of climate change during Heinrich events. Science 306, 2236–2239.
Konecky, B., Russell, J., Bijaksana, S., 2016. Glacial aridity in central Indonesia coeval with intensified monsoon circulation. Earth Planet Sci. Lett. 437, 15–24.
Konecky, B.L., Noone, D.C., Cobb, K.M., 2019. The influence of competing hydroclimate processes on stable isotope ratios in tropical rainfall. Geophys. Res. Lett. 46, 1622–1633.
Lee, T., Fournier, S., Gordon, A.L., Sprintall, J., 2019. Maritime Continent water cycle regulates low-latitude chokepoint of global ocean circulation. Nat. Commun. 10, 2103.
Li, Q., Wei, F., Li, D., 2011. Interdecadal variation of East Asian summer monsoon and drought/flood distribution over eastern China in the last 159 years. J. Geogr. Sci. 21, 579–593.
Li, C., Li, S., 2014. Interannual seesaw between the Somali and the Australian cross-equatorial flows and its connection to the East Asian summer monsoon. J. Clim. 27, 3966–3981.
Lisiecki, L.E., Stern, J.V., 2016. Regional and global benthic δ18O stacks for the last glacial cycle. Paleoceanography 31, 1368–1394.
Liu, Z., Harrison, S.P., Kutzbach, J., Otto-Bliesner, B., 2004. Global monsoons in the mid-Holocene and oceanic feedback. Clim. Dyn. 22, 157–182.
Ma, T., Chen, S., Chen, G., Zhou, X., Wang, Z., Zhao, K., Wang, Y., 2023. Synthesis of stalagmite climatic records in southern China during the last glacial-interglacial cycle. Quat. Int. 664, 1–12.
Marshall, A.G., Lynch, A.H., 2008. The sensitivity of the Australian summer monsoon to climate forcing during the late Quaternary. J. Geophys. Res. Atmos. 113, D11.
Martinez-Villalobos, C., Neelin, J.D., 2023. Regionally high risk increase for precipitation extreme events under global warming. Sci. Rep. 13, 5579.
Max, L., Nürnberg, D., Chiessi, C.M., Lenz, M.M., Mulitza, S., 2022. Subsurface ocean warming preceded Heinrich Events. Nat. Commun. 13, 4217.
Mersmann, O., Trautmann, H., Steuer, D., Bornkamp, B., 2023. truncnorm: truncated Normal distribution. R Package. CRAN R-project.org/package=truncnorm.
Miller, G., Mangan, J., Pollard, D., Thompson, S., Felzer, B., Magee, J., 2005. Sensitivity of the Australian Monsoon to insolation and vegetation: implications for human impact on continental moisture balance. Geology 33, 65–68.
Myers, N., Mittermeier, R.A., Mittermeier, C.G., Da Fonseca, G.A., Kent, J., 2000. Biodiversity hotspots for conservation priorities. Nature 403, 853–858.
Nilsson-Kerr, K., Anand, P., Holden, P.B., Clemens, S.C., Leng, M.J., 2021. Dipole patterns in tropical precipitation were pervasive across landmasses throughout Marine Isotope Stage 5. Commun. Earth Environ. 2, 64.
Oliveras, I., Malhi, Y., 2016. Many shades of green: the dynamic tropical forest–savanna transition zones. Phil. Trans. Biol. Sci. 371, 20150308.
Orihuela-Pinto, B., England, M.H., Taschetto, A.S., 2022. Interbasin and interhemispheric impacts of a collapsed Atlantic Overturning circulation. Nat. Clim. Change 12, 558–565.
Pei, R., Kuhnt, W., Holbourn, A., Hingst, J., Koppe, M., Schultz, J., Kopetz, P., Zhang, P., Andersen, N., 2021. Monitoring Australian Monsoon variability over the past four glacial cycles. Palaeogeogr. Palaeoclimatol. Palaeoecol. 568, 110280.
Piecuch, C.G., Beal, L.M., 2023. Robust weakening of the Gulf Stream during the past four decades observed in the Florida Straits. Geophys. Res. Lett. 50, e2023GL105170.
Pitman, A.J., Hesse, P.P., 2007. The significance of large-scale land cover change on the Australian palaeomonsoon. Quat. Sci. Rev. 26, 189–200.
Placzek, C.J., Quade, J., Patchett, P.J., 2013. A 130 ka reconstruction of rainfall on the Bolivian Altiplano. Earth Planet Sci. Lett. 363, 97–108.
Pontes, G.M., Menviel, L., 2024. Weakening of the Atlantic Meridional Overturning Circulation driven by subarctic freshening since the mid-twentieth century. Nat. Geosci. 17, 1291–1298.
Poulter, B., Frank, D., Ciais, P., Myneni, R.B., Andela, N., Bi, J., Broquet, G., Canadell, J. G., Chevallier, F., Liu, Y.Y., Running, S.W., 2014. Contribution of semi-arid ecosystems to interannual variability of the global carbon cycle. Nature 509, 600–603.
Qian, W., Shan, X., Chen, D., Zhu, C., Zhu, Y., 2012. Droughts near the northern fringe of the East Asian summer monsoon in China during 1470–2003. Clim. Change 110, 373–383.
Rowe, C., Brand, M., Hutley, L.B., Wurster, C., Zwart, C., Levchenko, V., Bird, M., 2019. Holocene savanna dynamics in the seasonal tropics of northern Australia. Rev. Palaeobot. Palynol. 267, 17–31.
Rowe, C., Wurster, C.M., Zwart, C., Brand, M., Hutley, L.B., Levchenko, V., Bird, M.I., 2021. Vegetation over the last glacial maximum at Girraween Lagoon, monsoonal northern Australia. Quaternary Research 102, 39–52.
Sarim, M., Xu, J., Zhang, P., Rahman, M.U., Iqbal, B., Qiao, J., Ke, F., Ran, Y., 2023. Late quaternary clay mineral and grain-size records from northwest Australia and their implications for paleoclimate, ocean currents, and paleodrainage of the Bonaparte basin. Palaeogeogr. Palaeoclimatol. Palaeoecol. 610, 111353.
Schaefer, J.M., Putnam, A.E., Denton, G.H., Kaplan, M.R., Birkel, S., Doughty, A.M., Kelley, S., Barrell, D.J., Finkel, R.C., Winckler, G., Anderson, R.F., 2015. The southern glacial maximum 65,000 years ago and its unfinished termination. Quat. Sci. Rev. 114, 52–60.
Scroxton, N., Gagan, M.K., Ayliffe, L.K., Hantoro, W.S., Hellstrom, J.C., Cheng, H., Edwards, R.L., Zhao, J.X., Suwargadi, B.W., Rifai, H., 2022. Antiphase response of the Indonesian–Australian monsoon to millennial-scale events of the last glacial period. Sci. Rep. 12, 20214.
Sekizawa, S., Nakamura, H., Kosaka, Y., 2021. Remote influence of the interannual variability of the Australian summer monsoon on wintertime climate in East Asia and the western North Pacific. J. Clim. 34, 9551–9570.
Sekizawa, S., Nakamura, H., Kosaka, Y., 2023. Interannual variability of the Australian summer monsoon sustained through internal processes: Wind–Evaporation feedback, dynamical air–sea interaction, and soil moisture memory. J. Clim. 36, 983–1000.
Shackleton, S., Baggenstos, D., Menking, J.A., Dyonisius, M.N., Bereiter, B., Bauska, T.K., Rhodes, R.H., Brook, E.J., Petrenko, V.V., McConnell, J.R., Kellerhals, T., 2020. Global ocean heat content in the Last Interglacial. Nat. Geosci. 13, 77–81.
Sharmila, S., Hendon, H.H., 2020. Mechanisms of multiyear variations of Northern Australia wet-season rainfall. Sci. Rep. 10, 1–11.
Singarayer, J.S., Valdes, P.J., Roberts, W.H., 2017. Ocean dominated expansion and contraction of the late Quaternary tropical rainbelt. Sci. Rep. 7, 9382.
Sun, C., Li, J., Jin, F.F., Ding, R., 2013. Sea surface temperature inter-hemispheric dipole and its relation to tropical precipitation. Environ. Res. Lett. 8, 044006.
Suppiah, R., 1992. The Australian summer monsoon: a review. Progress in Physical Geography 16, 283–318.
Veth, P., Smith, M., Bowler, J., Fitzsimmons, K., Williams, A., Hiscock, P., 2009. Excavations at Parnkupirti, Lake Gregory, great sandy desert: OSL ages for occupation before the last glacial maximum. Aust. Archaeol. 69, 1–10.

Wang, X., Auler, A.S., Edwards, R.L., Cheng, H., Cristalli, P.S., Smart, P.L., Richards, D. A., Shen, C.C., 2004. Wet periods in northeastern Brazil over the past 210 kyr linked to distant climate anomalies. Nature 432, 740–743.
Wang, L., Wen, C., Wen, Z., Gang, H., 2015. Drought in Southwest China: a review. Atmospheric and Oceanic Science Letters 8, 339–344.
Wang, P.X., Wang, B., Cheng, H., Fasullo, J., Guo, Z., Kiefer, T., Liu, Z., 2017. The global monsoon across time scales: mechanisms and outstanding issues. Earth Sci. Rev. 174, 84–121.
Williamson, G.J., Tng, D.Y., Bowman, D.M., 2024. Climate, fire, and anthropogenic disturbance determine the current global distribution of tropical forest and savanna. Environ. Res. Lett. 19, 024032.
van Westen, R.M., Kliphuis, M., Dijkstra, H.A., 2024. Physics-based early warning signal shows that AMOC is on tipping course. Sci. Adv. 10, eadk1189.
Wyrwoll, K.H., Miller, G.H., 2001. Initiation of the Australian summer monsoon 14,000 years ago. Quat. Int. 83, 119–128.
Wyrwoll, K.H., Valdes, P., 2003. Insolation forcing of the Australian monsoon as controls of Pleistocene mega-lake events. Geophys. Res. Lett. 30, 2279.
Wyrwoll, K.H., Liu, Z., Chen, G., Kutzbach, J.E., Liu, X., 2007. Sensitivity of the Australian summer monsoon to tilt and precession forcing. Quat. Sci. Rev. 26, 3043–3057.
Wyrwoll, K.H., Hopwood, J.M., Chen, G., 2012. Orbital time-scale circulation controls of the Australian summer monsoon: a possible role for mid-latitude Southern Hemisphere forcing? Quat. Sci. Rev. 35, 23–28.
Xu, X., Medvigy, D., Trugman, A.T., Guan, K., Good, S.P., Rodriguez-Iturbe, I., 2018. Tree cover shows strong sensitivity to precipitation variability across the global tropics. Global Ecol. Biogeogr. 27, 450–460.
Xu, D., Lu, H., Chu, G., Shen, C., Sun, Q., Wu, J., Li, F., Song, B., Cui, A., Li, H., Wu, N., 2023. Fast response of vegetation in East Asia to abrupt climatic events during the last deglaciation. PNAS Nexus 2, pgad061.
Xue, J., Wang, B., Yu, Y., Li, J., Sun, C., Mao, J., 2022. Multidecadal variation of northern hemisphere summer monsoon forced by the SST inter-hemispheric dipole. Environ. Res. Lett. 17, 044033.
Yeung, N.K.H., Menviel, L., Meissner, K.J., Taschetto, A.S., Ziehn, T., Chamberlain, M., 2021. Land–sea temperature contrasts at the last Interglacial and their impact on the hydrological cycle. Clim. Past 17, 869–885.
Yu, Y., Notaro, M., 2020. Observed land surface feedbacks on the Australian monsoon system. Clim. Dyn. 54, 3021–3040.
Zhang, R., Delworth, T.L., 2005. Simulated tropical response to a substantial weakening of the Atlantic thermohaline circulation. J. Clim. 18, 1853–1860.
Zhang, W., Zhou, T., Zou, L., Zhang, L., Chen, X., 2018. Reduced exposure to extreme precipitation from 0.5 C less warming in global land monsoon regions. Nat. Commun. 9, 3153.
Zhang, P., Xu, J., Holbourn, A., Kuhnt, W., Beil, S., Li, T., Xiong, Z., Dang, H., Yan, H., Pei, R., Ran, Y., 2020. Indo-Pacific hydroclimate in response to changes of the intertropical convergence zone: discrepancy on precession and obliquity bands over the last 410 kyr. J. Geophys. Res. Atmos. 125, e2019JD032125.
Zhao, D., Lu, Z., Wan, S., Cheng, H., Shi, X., Li, A., 2023. Quaternary rainfall variability is governed by insolation in northern China and ice-sheet forcing in the South. Commun. Earth Environ. 4 (1), 7.
Zwart, C., Munksgaard, N.C., Protat, A., Kurita, N., Lambrinidis, D., Bird, M.I., 2018. The isotopic signature of monsoon conditions, cloud modes, and rainfall type. Hydrol. Process. 32, 2296–2303.